Research Article | Vol. 27, No. 13 | 24 Jun 2019 | OPTICS EXPRESS 18410
Optics EXPRESS

Symmetry selective cladding modes coupling in ultrafast-written fiber Bragg gratings in two-mode fiber

DINGYI FENG,[1,*] JACQUES ALBERT,[2] YAJUN JIANG,[1,4] CHI LIU,[1] BIQIANG JIANG,[1] HAOYUN WANG,[3] AND JIANLIN ZHAO[1]

[1]*MOE Key Laboratory of Space Applied Physics and Chemistry and Shaanxi Key Laboratory of Optical Information Technology, School of Science, Northwestern Polytechnical University, Xi'an 710072, China*
[2]*Department of Electronics, Carleton University, Ottawa, Ontario, K1S 5B6, Canada*
[3]*Petrochina Southwest Pipeline Company, Tianshui, Gansu, 741000, China*
[4]*yjjiang@nwpu.edu.cn*
**fengdingyi@nwpu.edu.cn*

Abstract: The lower order cladding mode resonances of a fiber Bragg grating (FBG) are sensitive to fiber bending but their spectral density makes their response to bending very complex. In this work we present a simple method to reduce and control the number of low order cladding mode resonances via FBGs written in a two-mode fiber (TMF) with an ultrafast laser. Owing to the larger core size of the TMF, a slight break of the cylindrical asymmetry of the grating patterns can be induced when using femtosecond side-irradiation with a small change in the writing condition. This allows us to control the mode families coupled by the grating, and in particular to those modes that have positive or negative bending responses along certain bend directions. Experimental results demonstrate that several lower-order neighboring-cladding mode pairs coupled by the asymmetric TMFBG have antagonistic loss responses (by several dB) for different bending directions, thus allowing full 2D bending measurements with many applications in shape sensing. Finally, this device has similar advantages as tilted FBGs, i.e. temperature de-correlation and the possibility of increasing the signal to noise ratio by averaging simultaneous measurements on several pairs of resonances.

1. Introduction

The ability to quantify the deformation/shape of an object by measuring the magnitude and direction of bends at certain points can help to evaluate its structural integrity in real time and it is vital in various large engineering applications. Fiber-optic bend sensors are ideally suited for this task because they can be integrated seamlessly and in large numbers. In the past decades, a few modal-interference-based bend sensors have been demonstrated [1–5], and, in most cases, fiber mismatches/discontinuities (like lateral-offset splicing [6] and tapers [7]) or specialty fibers with asymmetric structures [2,8–10] are introduced to recognize different bending planes. Simpler directional bending schemes have also been reported by adding additional fiber waveguides [11,12]. However, for all fiber interferometers light source and loss power fluctuations and cross-sensitivities of other parameters (temperature in particular) remain problematic to deal with. Additionally, discontinuous fiber structures are somewhat complicated (and costly) to assemble and less robust. In order to address some of these issues, there has been a number of recent reports where off-axis gratings in multi-core fibers were used [13–15]. Such configurations enable gratings to sense differential bending-caused off-axis strains and thus to reconstruct shape deformations, but they come with additional issues related to the uniformity of co-located gratings written in multi-core geometries and the cost of multiplexing and demultiplexing light across the cores.

#364317 https://doi.org/10.1364/OE.27.018410
Journal © 2019 Received 5 Apr 2019; revised 21 May 2019; accepted 27 May 2019; published 17 Jun 2019

Optics EXPRESS

While fiber gratings written in the core of single mode fibers are insensitive to pure bending, any form of symmetry breaking dramatically changes the transmitted spectra for co-propagating (long period grating (LPG)) or counter-propagating (fiber Bragg grating (FBG)) interactions, and results in the excitation of cladding modes with resonance wavelengths and amplitudes that depend on fiber bending [16–22]. Asymmetrical LPGs, such as sector-shaped [17], V-shaped [20] and oppositely tilted LPGs [21], can show strong directional-bending responses, but LPGs are notoriously highly sensitive to the surrounding temperature as well as the refractive index change of the external medium, which will inevitably affect the measurement accuracy. For FBGs however, these effects can be calibrated out by measuring the wavelength and amplitude of the core mode reflection Bragg resonance that is essentially insensitive to fiber bend and external index [16,23–25]. An especially simple way to break the azimuthal symmetry of a FBG is to tilt the grating planes [26–28]. A tilted FBG (TFBG) based on small-core fiber has been proposed with a maximal bending response of –0.17 dB/m^{-1} (according to different bending orientations) [26]. Also, in previous publications from our group an orthogonal TFBG-pair structure [27] and an off-axis FBG [16] have been proposed. And through using simple power level detection of well-selected lower-order cladding modes, "directional" bending sensitivities of 0.3 dB/m^{-1} and 1.3 dB/m^{-1} were obtained. In another method, the symmetry of FBGs can be broken by writing "localized" FBGs with an ultrafast laser so that the refractive index modulation is limited to a small fraction of the core cross-section, leading to the excitation of cladding resonances and to symmetry breaking in the same manner as with TFBGs [29,30]. However, nontrivial modification and precise alignment of grating writing tools are required in such processing such structures. Finally, several other vector bending schemes have also been investigated with FBGs in and eccentric-core [31] and D-shaped fibers [32], for which low loss splicing to standard single mode fiber (SMF) is difficult.

In this paper we propose and demonstrate a novel and much simpler approach of slightly breaking the cylindrical symmetry of an FBG. The grating is written in a two-mode fiber (TMF) that has a much larger core size than the standard SMF. The technique demonstrated is based on the process of femtosecond laser side-irradiation via a phase mask (PM) but with an addition of a very small adjustment of the PM/TMF distance. The grating fringes in a TMFBG are then much stronger on one side of the core than on the other. As a result, while the centered grating couples exclusively to cladding modes of the same azimuthal symmetry, the displaced one also couples to mode families with other symmetries. We further compare the bending responses of the asymmetric grating with a centered one that has been developed earlier by our group in the same fiber [33], and find that the transmitted spectral amplitudes of several pairs of well-separated but neighboring cladding resonances in a TMFBG alternatively increase or decrease, depending on the bend orientations relative to the asymmetrical distribution plane of the grating refractive index. This allows us to use the relative power level changes between two neighboring cladding modes to quantify the bend magnitude and direction, and enable the grating to act as a full directional bending sensor with much higher sensitivity. The occurrence of this phenomenon over many such pairs of resonances also provides a way to improve the signal to noise ratio by averaging the calibrated responses from several resonance pairs. Compared with previous works, the proposed approach simplifies the fabrication of an asymmetric grating and improves the accuracy of the measurement for vector bending. It also provides an efficient way for us to make a 3D shape sensor that could find applications in structural health monitoring of large structures such as bridges, buildings, oil pipeline, airplane wings and smart robots.

Optics EXPRESS

2. Fabrication and characterization

2.1 Grating fabrication

Figure 1 shows the schematic diagram of the TMFBG fabrication. The TMF has core/cladding diameters of 20/125 μm and refractive index difference of 0.32% (OFS, Item#60816). The fiber is hydrogen-loaded at 10 MPa for two weeks prior to grating fabrication order to increase the fiber photo-sensitivity (the laser intensity threshold for grating formation is significantly reduced as a consequence). The TMFBG inscription procedure is shown in Fig. 1(a). A femtosecond pulse from a 800 nm-wavelength Ti:sapphire amplifier (Spectra-physics SPFIRE ACE-35F-1KXP) is used as a light source to deliver pulses with 35 fs duration and 4 mJ of energy at a 1 kHz repetition rate. A half-wave plate and a polarizer located at the laser output are used to adjust output pulse energy. A cylindrical lens with a focal length of 40 mm is used to focus the laser beam that is imaged onto the fiber through a diffractive PM (Ibsen Photonics) with a period of 2.142 μm to obtain the periodic intensity patterns (for this mask period, the second order resonance of the in-fiber grating is phase-matched at the optical wavelengths used). Under these conditions a TMFBG can be inscribed by precisely adjusting the distance between the TMF and the PM located in close proximity to it.

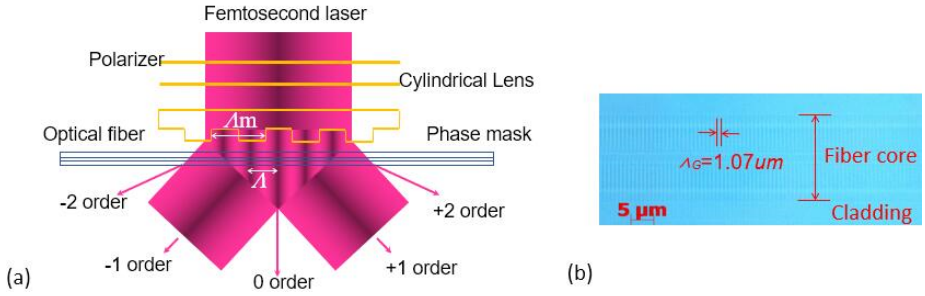

Fig. 1. Schematic diagrams of (a) the TMFBG inscription by femtosecond laser and (b) the phase contrast microscope image of the TMFBG2, respectively.

Here, we name the centered and the offset grating as TMFBG1 and TMFBG2, respectively. TMFBG1 is written under the same condition as that in [33]. By contrast, what we find so interesting is that when slightly adjusting the distance of the fiber to the PM, and increasing the laser pulse (but not beyond the energy range for efficient grating formation), TMFBG2 with a quite different transmitted spectrum is formed (as shown below in Fig. 2). Figure 1(b) further shows a phase contrast microscope image of the refractive index pattern in TMFBG2. It indicates that the grating fringes with a period of 1.071 μm (half the pitch of the PM) cover the whole cross-section of the fiber core (therefore not "off-axis" or "localized" as that in [16] and [29]). The fiber-PM distance adjustment required for the formation of TMFBG2 is determined empirically by observing changes in the diffraction pattern of the laser going through the fiber on a screen located behind the fiber: i.e. just when the edge of the diffraction pattern loses sharpness. While this criterion is not 100% reproducible, upon verification and several additional gratings produced, it is possible to identify in the transmission spectrum of TFBGs the features associated with the required asymmetry and thus to select the "good" ones unambiguously. Since the eventual sensitivity deviates slightly from grating to grating, a calibration of each sensor is required prior to use. We further explain the difference gratings TMFBG1 and TMFBG2 by the fact that as the laser is side-irradiated to the so large core of the TMF, a very small change of the position of TMF and higher intensity exposure can cause a very small index change gradient along the laser beam propagation direction, thus creating a slight asymmetry. This hypothesis is supported by the bending results reported further in this paper.

Optics EXPRESS

2.2 Spectral analysis

The proposed gratings are spliced to the standard SMF on both ends by a fiber splicer (Fujikura FSM-60S) in "auto splicing mode" (the estimated splicing loss is about 0.1 dB), and then connected to a broadband light source (BBS) (Exfo, FLS-2300B) and an optical spectrum analyzer (OSA) (Yokogawa, AQ6370) with a resolution of 0.01nm. The transmitted spectra of the two gratings are reproduced in Fig. 2. It can be seen that TMFBG1 and TMFBG2 both exhibit strong Bragg reflectivities at 1550.21 nm and 1547.97 nm, corresponding to the two guided core modes, LP_{01} and LP_{11} respectively. And it is the 2nd order grating that inscribed in TMF according to the Bragg equation of $m\lambda_i = 2n_{eff,i}\Lambda_G$, where λ_i is the wavelength of *ith* core mode, m is the order number, and $n_{eff,i}$ is the effective index of the *ith* core modes (i = 1 and 2, in the case of TMFBG). The core mode fields are limited to the fiber core and theoretically insensitive to external bending (because they lie on the zero strain axis of the fiber cross section).

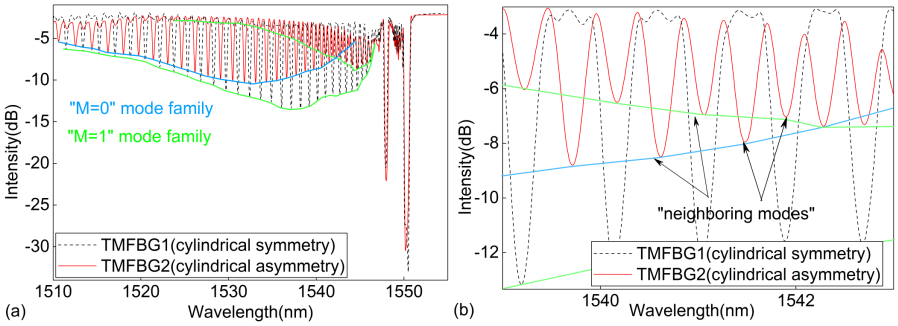

Fig. 2. (a) Transmitted spectrum comparison of the proposed TMFBGs under two different writing conditions and (b) the zoomed-in multi-pairs of neighboring modes.

In addition, combs of cladding mode resonances over a bandwidth of ~30 nm are also present in both spectra, indicating the strong coupling between cladding modes and the core modes in gratings. However, the spectral envelopes of TMFBG1 and TMFBG2 are quite different. According to Fig. 2 (a) we see the drawn lines for the envelopes of different mode families coupled by the gratings. For TMFBG1, the index perturbation is well centered (cylindrical symmetry), so the incident core mode (LP_{01}, i.e. HE_{11}) only couples to cladding modes of the same azimuthal "family" (HE_{1M} modes, here since the weakly guiding approximation no longer applies for cladding modes guided by a glass-air boundary) according to coupled-mode theory [34,35], so there is a single envelope (marked by green line and labeled "M=1") corresponding to the symmetric fiber mode family. For the TMFBG2 spectrum, in addition to amplitude changes of the resonances, new resonances appear between the ones of TMFBG1 (with an envelope marked by a blue line and labeled "M=0"). As shown in [36] these correspond to modes with even M numbers (0, 2, 4 ...) and must be due to an asymmetry of the perturbation in the azimuthal direction. The presence of these two mode families in TMFBG2 thus forms multi-pairs of "neighboring modes" with halved spectral spacing in the wavelength range from 1539 nm to 1543 nm, as shown in the zoomed-in spectra of Fig. 2(b). It is these well-defined lower order pairs of modes that can be employed for high-quality measurement of the curvature as well as of the determination of the bend direction.

3. Experiments and results

The bending sensor is characterized with the same setup as in [16]. As is shown in Fig. 3, a section of TMF with a length of 25 cm is bent with controlled radii along all possible directions by fixing the inscribed grating exactly in the middle of a set of standard translation

Optics EXPRESS

stages with two rotating holders. The curvature C (defined as the inverse of bending radius R) is calculated by $C = 2h/[h^2 + (L/2)^2]$, where L and h are the distance of the fixed points and the central vertical displacement of the grating, respectively. As it is known that bending of a fiber induces a refractive index perturbation that depends linearly on the distance from fiber axis, with a value of zero at the center and increasing/decreasing on the inside/outside of the bend, the coupling coefficients to cladding modes change accordingly [37]. Here, for the still symmetric TMFBG1, bending is expected to shift the centers of the mode patterns in the direction of the bend and to cause a decrease of the coupling to modes of the M = 1 family (as well as to some very weak coupling to modes of the M = 0 family since the bend-induced refractive index is asymmetric). For the inherently asymmetric TMFBG2 the coupling to M = 0 and M = 1 mode family will either increase or decrease, depending on the angles between the bend plane and the grating-induced refractive index offset. To verify these points the two types of gratings are characterized for bending.

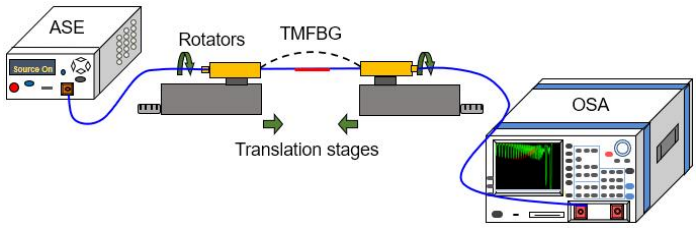

Fig. 3. Schematic diagram of the experimental setup for vector bend testing.

Figure 4 shows the transmitted spectra of the TMFBG2 for a series of curvature values C at a fixed bending plane orientation. The interval between the curvature values is set at $0.135 m^{-1}$. It is confirmed that the two Bragg resonances are immune to change under these curvatures but that the cladding resonances show significant intensity changes of several dB: the amplitude of the transmission loss dips located at 1539.7 nm, 1540.6 nm, and 1541.5nm clearly decreased with increasing curvature from 0 to 1.35 m^{-1}; on the contrary, their neighboring resonances located at 1540.2 nm, 1541.1nm and 1541.9 nm all increased. This confirms that these two groups of resonances belong to different mode families that respond independently to external bending. In order to quantify the bending sensitivity, a pair of strong neighboring cladding mode resonances located at 1540.7 nm and 1541.1 nm are selected as they are the most bend-sensitive pair for this range of curvatures, as shown in the inset of Fig. 4.

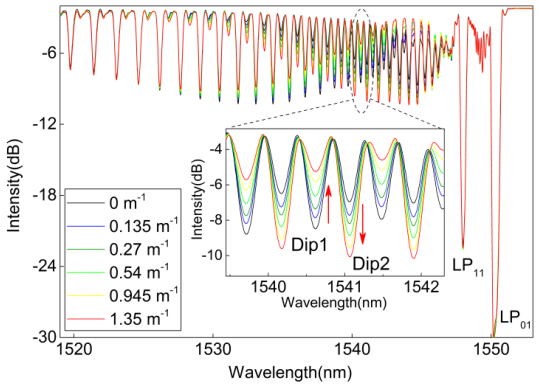

Fig. 4. Transmission spectra of TMFBG2 for various curvatures. The inset show the zoomed bending-induced responses of the cladding mode resonances from 1539 nm to 1542 nm.

Optics EXPRESS

Before testing the bending sensitivity quantitatively, the input polarization state effect on the transmission spectra of both types of gratings is studied in order to eliminate polarization-induced effects such as those observed for higher order modes of TFBGs [36]. A polarizer and a polarization controller are connected to the light source for these measurements. The capture of the sensor spectra under two orthogonal polarizations (arbitrarily labeled TE and TM) is shown in Fig. 5. It can be seen that the low order cladding resonances for both TMFBG1 and TMFBG2 (with a centered and offset equivalent center, as shown the sketches in inserts of Fig. 5(a) and 5(b)) present a negligible polarization splitting. Additionally, the bending responses under TE- and TM- polarization are almost the same as those obtained with un-polarized light in Fig. 4. Therefore, un-polarized light can be (and will be) used in our experiments.

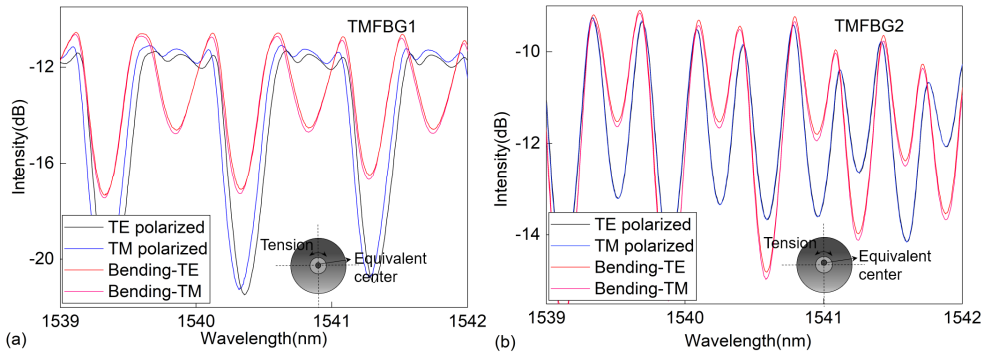

Fig. 5. The spectral comparisons of (a) TMFBG1 and (b) TMFBG2 from 0 m^{-1} to 1 m^{-1} under TE-, and TM-polarization states, respectively. The inserts indicate the equivalent center of the two grating patterns.

Figure 5 also shows sketches of how the "equivalent" center of TMFBG2 is displaced and the orientation (vertical, in the same direction as the fiber-PM displacement used for writing the TMFBG2) of the bend plane used for these spectrum measurements (giving rise to tensile (top) and compressive (bottom) stresses across the fiber section).

Optics EXPRESS

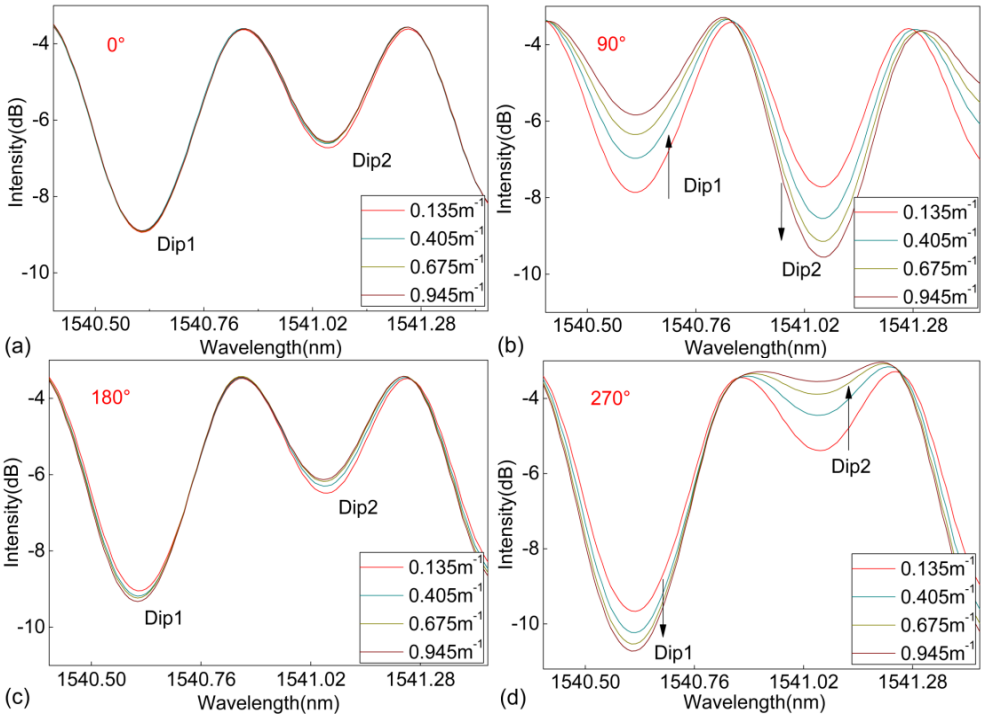

Fig. 6. The changes of the selected neighboring cladding resonances for bending orientations of (a) 0°, (b) 90°, (c)180°, and (d)270°, respectively.

Figure 6 indicates how the coupling strengths of the selected pair of resonances (labeled Dip1 and Dip2) vary for different bend magnitudes and orientations. It is clear from Figs. 6(a) and 6(c) that the amplitudes of both resonances are invariable under different curvature values *C* when the bending plane is located at 0° and 180°, respectively. On the other hand, as the bending plane is rotated to 90°, Dip1 is decreases continuously with increasing of *C*, while its neighboring Dip2 increases by an almost exactly equal amount. And when bending occurs in the precisely opposite direction (270°), the amplitude changes of these two resonances both reverse sign as expected (Figs. 6(b) and 6(d)).

A typical set of bending results for the same two dips are thus obtained by measuring the amplitudes of the selected dips for various values of the curvature for different bending azimuthal orientations between 0° and 360° around the fiber axis at an interval of 30°. It is clear from Fig. 7 that the amplitude variations for both dips are linear with curvature *C* from 0 to 1.35 m^{-1}. And the bending sensitivities vary from –1.92 dB/m^{-1} at 90° to + 2.58 dB/m^{-1} at 270° for Dip1 in Fig. 7(a), and from + 2.54 dB/m^{-1} to –2.11 dB/m^{-1} for Dip2 in Fig. 7(b), respectively. In addition, the two insets in Fig. 7 show that the intensity responses for Dip1 and Dip2 are both approximately sinusoidal with bend orientation and exactly out of phase by half a period. As a result, we can also use these two dips in a single TMFBG to remove the uncertainty in the bend plane and thus determine the bend orientation (similar to our previous work in [27]), so that a true 3D shape sensing can be realized with the addition of axial strain measurement. Additionally, instead of considering the individual amplitudes of the two dips, we can choose to use their relative amplitude and the bend sensing results are independent of light source power or insertion loss variations.

Optics EXPRESS

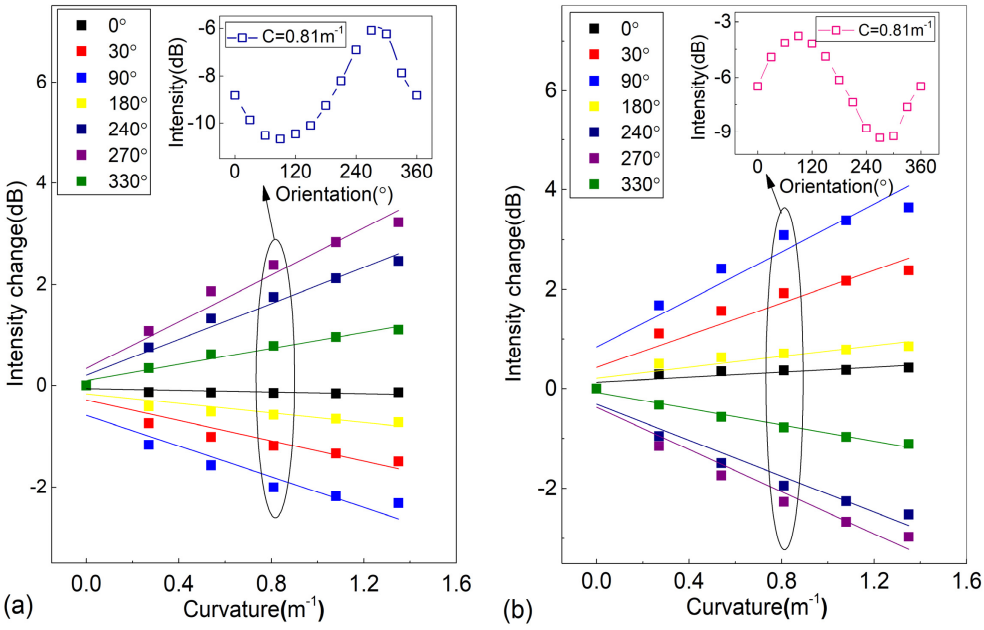

Fig. 7. Bending orientation dependence of the selected cladding mode of Dip1 (a) and Dip2 (b) under different curvatures with linear fits.

This is shown in Fig. 8 for the response of the relative intensity change of two dips as a function of bend orientations. It is clear from the sine-fitted curve that the maximum sensitivities are achieved for −5.23 dB/m^{-1} and + 4.68 dB/m^{-1}, separately, with a 180° phase difference, which are greatly enhanced compared to the maximum values of 0.17 and 1.25 dB/m^{-1}, in [26] and [27], and 1.9 dB/m^{-1} in [16].

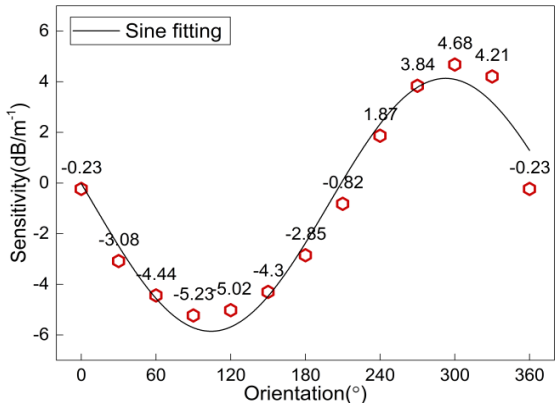

Fig. 8. Sensitivities of the relative amplitude changes of selected cladding dips versus bend orientations from 0° to 360°.

For comparison, TMFBG1 is also tested under different bend directions. Figure 9 shows the spectral changes of this azimuthally symmetric grating under a curvature C = 0.81 m^{-1} with bend planes at 0°, 90°, 180° and 270°, respectively. It can be seen that when the fiber is bent in the two horizontal directions (0° and 180°) no obvious change occurs. But when the fiber is bent in the vertical directions (90° and 270°) the amplitude of the main M = 1 modes are decreased, meanwhile, some new neighboring mode resonances (corresponding to the M = 0 mode family) appear and increase as bending creates an asymmetry due to the non-

Optics EXPRESS

uniform compression/extension of the grating pattern, as mentioned above. Compared to the changes of dip amplitude for TMFBG2 in Fig. 6, the dependence of bending orientation for TMFBG1 is only half the periodicity due to the strictly positive or negative changes for the dips (to be precise, here the only asymmetry is the one introduced by the bending whereas in TMFBG2 the bending induced asymmetry either helps or compensates for the grating induced asymmetry). As a result, with TMFBG1 the direction within the bending plane (up or down) is uncertain.

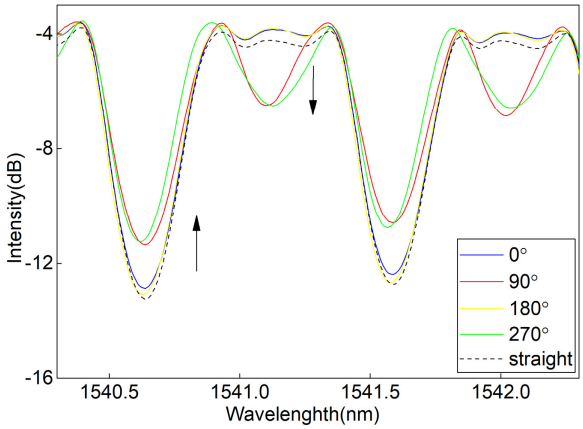

Fig. 9. Spectral changes of the centered TMFBG1 under different bend planes.

Lastly, a separate measurement is carried out for TMFBG2 to study the temperature cross-sensitivity. As shown in Fig. 10, an increase of the temperature causes a red-shift of the overall spectra with negligible shape variation. The zoomed-in spectra in the inset of Fig. 10(a) indicates that the amplitudes of the selected dips are almost invariable. More detailed measurements in Fig. 10(b) show that the intensity fluctuations are within ± 0.03 dB for both resonances for temperatures ranging from 21.8 to 61.5°C, while their wavelengths shift with a sensitivity of ~9.6 pm/°C, the same value as that of the core mode resonances (which can be measured simultaneously to determine the temperature *in situ* and, if needed, to adjust the detection system to "follow" the pairs of resonances used for the bend measurement. Therefore, the measurements of vector bending can be made regardless of temperature since they rely on power level detection only.

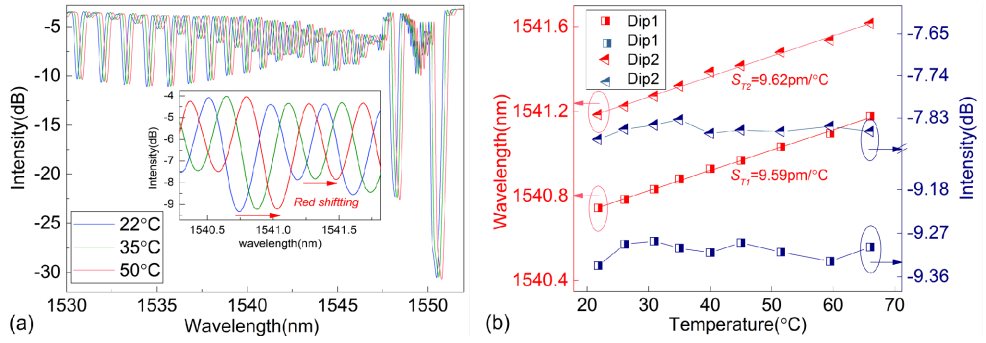

Fig. 10. (a) Spectra responses of TMFBG2 under different temperatures. Insert indicates the zoomed-in resonances used for bend measurement; (b) Wavelength shifts and intensity fluctuations versus temperature, respectively.

Optics EXPRESS

4. Conclusion

In conclusion, we have introduced a new method for slightly breaking the cylindrical symmetry of an optical fiber with a larger core able to support two modes by writing a FBG with an ultrafast laser system and a phase mask slightly separated from the fiber. The bending response of the standard (centered) and asymmetric TMFBGs for lower-order cladding modes have confirmed that this technique creates a symmetry axis in the fiber and that pairs of cladding mode resonances change amplitude in opposite directions and with a magnitude that depends on bending magnitude and direction. Relative power measurements of these two amplitudes reveal directional bend sensitivities greater than 4 dB/m^{-1} over curvatures ranging from 0 to 1.35 m^{-1}, and immunity to power level fluctuations (since the measurement is a relative one, between spectrally neighboring resonances). The magnitude of the bend sensitivity varies sinusoidally with bend orientation over a full 360 rotation. This device is simple in fabrication, without having to de-localize or offset gratings from the core center, it is easy to splice to standard SMF, yet it provides high vector bend sensitivities with power level interrogation.

Funding

National Natural Science Foundation of China (NSFC) (61705185, 61775182); Natural Science Basic Research Program of Shaanxi (2018JQ6101, 2019JM-076); Aeronautical Science Foundation of China (ASFC) (2016ZD53039); Research Funds for the Central Universities (31020170QD062, 3102017jghk02011).

References

1. A. V. Newkirk, J. E. Antonio-Lopez, A. Velazquez-Benitez, J. Albert, R. Amezcua-Correa, and A. Schülzgen, "Bending sensor combining multicore fiber with a mode-selective photonic lantern," Opt. Lett. **40**(22), 5188–5191 (2015).
2. K. Naeem, Y. Chung, and I. Kwon, "Highly sensitive two-dimensional bending vector sensor using an elliptic two-core PCF," IEEE Photonics Technol. Lett. **30**(3), 273–276 (2018).
3. S. Wang, Y. X. Zhang, W. G. Zhang, P. C. Geng, T. Y. Yan, L. Chen, Y. P. Li, and W. Hu, "Two-dimensional bending vector sensor based on the multimode-3-core-multimode fiber structure," IEEE Photonics Technol. Lett. **29**(10), 822–825 (2017).
4. K. Tian, Y. Xin, W. Yang, T. Geng, J. Ren, Y. Fan, G. Farrell, E. Lewis, and P. Wang, "A curvature sensor based on twisted single-mode–multimode–single-mode hybrid optical fiber structure," J. Lightwave Technol. **35**(9), 1725–1731 (2017).
5. H. Gong, D. Wang, M. Xiong, C. Zhao, and K. Ni, "Optical fiber hollow ellipsoid for directional bend sensing with a large bending range," Opt. Mater. Express **7**(6), 1767–1776 (2017).
6. S. Zhang, W. Zhang, S. Gao, P. Geng, and X. Xue, "Fiber-optic bending vector sensor based on Mach-Zehnder interferometer exploiting lateral-offset and up-taper," Opt. Lett. **37**(21), 4480–4482 (2012).
7. L. Zhang, W. Zhang, L. Chen, T. Yan, L. Wang, B. Wang, and Q. Zhou, "A fiber bending vector sensor based on M–Z interferometer exploiting two hump-shaped tapers," IEEE Photonics Technol. Lett. **27**(11), 1240–1243 (2015).
8. C. Kong, X. Ouyang, A. Zhou, and L. Yuan, "Highly sensitive directional bending sensor based on eccentric core fiber Mach–Zehnder modal interferometer," IEEE Sens. J. **16**(18), 6899–6902 (2016).
9. R. Gao, D. Lu, J. Cheng, and Z. M. Qi, "Self-referenced antiresonant reflecting guidance mechanism for directional bending sensing with low temperature and strain crosstalk," Opt. Express **25**(15), 18081–18091 (2017).
10. H. Chen, Y. Wang, and D. Wang, "Selectively infiltrated PCF for directional bend sensing with large bending range," IEEE Photonics Technol. Lett. **27**(5), 502–505 (2015).
11. D. Pallarés-Aldeiturriaga, L. Rodríguez-Cobo, A. Quintela, and J. M. López-Higuera, "Curvature sensor based on in-fiber Mach–Zehnder interferometer inscribed with femtosecond laser," J. Lightwave Technol. **35**(21), 4624–4628 (2017).
12. S. Li, Z. Wang, Y. Liu, T. Han, Z. Wu, C. Wei, H. Wei, J. Li, and W. Tong, "Bending sensor based on intermodal interference properties of two-dimensional waveguide array fiber," Opt. Lett. **37**(10), 1610–1612 (2012).
13. S. Wang, W. Zhang, L. Chen, Y. Zhang, P. Geng, Y. Zhang, T. Yan, L. Yu, W. Hu, and Y. Li, "Two-dimensional microbend sensor based on long-period fiber gratings in an isosceles triangle arrangement three-core fiber," Opt. Lett. **42**(23), 4938–4941 (2017).
14. M. Hou, K. Yang, J. He, X. Xu, S. Ju, K. Guo, and Y. Wang, "Two-dimensional vector bending sensor based on seven-core fiber Bragg gratings," Opt. Express **26**(18), 23770–23781 (2018).

Optics EXPRESS

15. D. Barrera, J. Madrigal, and S. Sales, "Long period gratings in multicore optical fibers for directional curvature sensor implementation," J. Lightwave Technol. **36**(4), 1063–1068 (2018).
16. D. Feng, X. Qiao, and J. Albert, "Off-axis ultraviolet-written fiber Bragg gratings for directional bending measurements," Opt. Lett. **41**(6), 1201–1204 (2016).
17. Q. Zhou, W. Zhang, L. Chen, Z. Bai, L. Zhang, L. Wang, B. Wang, and T. Yan, "Bending vector sensor based on a sector-shaped long-period grating," IEEE Photonics Technol. Lett. **27**(7), 713–716 (2015).
18. P. Saffari, T. Allsop, A. Adebayo, D. Webb, R. Haynes, and M. M. Roth, "Long period grating in multicore optical fiber: an ultra-sensitive vector bending sensor for low curvatures," Opt. Lett. **39**(12), 3508–3511 (2014).
19. J. Kong, A. Zhou, C. Cheng, J. Yang, and L. Yuan, "Two-axis bending sensor based on cascaded eccentric core fiber Bragg gratings," IEEE Photonics Technol. Lett. **28**(11), 1237–1240 (2016).
20. Y. Zhang, W. Zhang, T. Yan, L. Bie, Y. Zhang, S. Wang, L. Kong, X. Kang, L. Yu, and P. Geng, "V-shaped long-period fiber grating high-sensitive bending vector sensor," IEEE Photonics Technol. Lett. **30**(17), 1531–1534 (2018).
21. Y. Li, W. Zhang, S. Wang, L. Chen, Y. Zhang, B. Wang, T. Yan, X. Li, and W. Hu, "Bending vector sensor based on a pair of opposite tilted long-period fiber gratings," IEEE Photonics Technol. Lett. **29**(2), 224–227 (2017).
22. W. Ni, P. Lu, C. Luo, X. Fu, L. Liu, H. Liao, X. Jiang, D. Liu, and J. Zhang, "Bending direction detective fiber sensor for dual-parameter sensing based on an asymmetrical thin-core long-period fiber grating," IEEE Photonics J. **8**(4), 6803811 (2016).
23. W. Bao, X. Qiao, Q. Rong, N. Hu, H. Yang, Z. Feng, and M. Hu, "sensing characteristics for a fiber Bragg grating inscribed over a fiber core and cladding," IEEE Photonics Technol. Lett. **27**(7), 709–712 (2015).
24. S. Baek, Y. Jeong, and B. Lee, "Characteristics of short-period blazed fiber Bragg gratings for use as macro-bending sensors," Appl. Opt. **41**(4), 631–636 (2002).
25. K. Yang, J. He, C. Liao, Y. Wang, S. Liu, K. Guo, J. Zhou, Z. Li, Z. Tan, and Y. Wang, "Femtosecond laser inscription of fiber Bragg grating in twin-core few-mode fiber for directional bend sensing," J. Lightwave Technol. **35**(21), 4670–4676 (2017).
26. L. Shao, L. Xiong, C. Chen, A. Laronche, and J. Albert, "Directional bend sensor based on re-grown tilted fiber Bragg grating," J. Lightwave Technol. **28**(18), 2681–2687 (2010).
27. D. Feng, W. Zhou, X. Qiao, and J. Albert, "Compact optical fiber 3D shape sensor based on a pair of orthogonal tilted fiber Bragg gratings," Sci. Rep. **5**(1), 17415 (2015).
28. B. Jiang, K. Zhou, C. Wang, Q. Sun, G. Yin, Z. Tai, K. Wilson, J. Zhao, and L. Zhang, "Label-free glucose biosensor based on enzymatic graphene oxide-functionalized tilted fiber grating," Sens. Actuators B Chem. **254**, 1033–1039 (2018).
29. J. Thomas, N. Jovanovic, R. G. Becker, G. D. Marshall, M. J. Withford, A. Tünnermann, S. Nolte, and M. J. Steel, "Cladding mode coupling in highly localized fiber Bragg gratings: modal properties and transmission spectra," Opt. Express **19**(1), 325–341 (2011).
30. J. U. Thomas, N. Jovanovic, R. G. Krämer, G. D. Marshall, M. J. Withford, A. Tünnermann, S. Nolte, and M. J. Steel, "Cladding mode coupling in highly localized fiber Bragg gratings II: complete vectorial analysis," Opt. Express **20**(19), 21434–21449 (2012).
31. W. Bao, Q. Rong, F. Chen, and X. Qiao, "All-fiber 3D vector displacement (bending) sensor based on an eccentric FBG," Opt. Express **26**(7), 8619–8627 (2018).
32. B. Jiang, Z. Bai, C. Wang, Y. Zhao, J. Zhao, L. Zhang, and K. Zhou, "In-line Mach-Zehnder interferometer with D-shaped fiber grating for temperature-discriminated directional curvature measurement," J. Lightwave Technol. **36**(3), 742–747 (2018).
33. Y. Jiang, C. Liu, W. Zhang, D. Mao, D. Yang, and J. Zhao, "Multi-parameter sensing using a fiber Bragg grating inscribed in dual-mode fiber," IEEE Photonics Technol. Lett. **29**(19), 1607–1610 (2017).
34. A. Othonos and K. Kalli, *Fiber Bragg gratings* (Artech House, 1999).
35. T. Erdogan, "Cladding-mode resonances in short- and long period fiber grating filters," J. Opt. Am. A **14**(8), 1760–1773 (1997).
36. M. Z. Alam and J. Albert, "Selective excitation of radially and azimuthally polarized optical fiber cladding modes," J. Lightwave Technol. **31**(19), 3167–3175 (2013).
37. U. Block, M. Digonnet, M. Fejer, and V. Dangui, "Bending-induced birefringence of optical fiber cladding modes," J. Lightwave Technol. **24**(6), 2336–2339 (2006).